Study of electrostatic potential induced by friction

Shiyu Hu, Yuanyue Zhang, Tianmin Shao*
State Key Lab of Tribology, Tsinghua University
shaotm@tsinghua.edu.cn 86-10-62783160

***Abstract*—Electrostatic potential during friction between two kinds of stainless steels was measured. Result shows a direct correlation between electrostatic potential and friction coefficient. Influence of normal load, sliding speed and surface roughness on electrostatic potential was studied. Wear tracks and wear debris were studied by using a scanning electron microscope (SEM) and Energy Dispersive X-ray (EDX). It was found that friction coefficient, electrostatic potential and the extent of oxidation are closely correlated, indicated the difference in wear mechanisms for the three stages. Samples with different thickness of surface oxidization were prepared to study the influence of the oxidation layer. Results show that both fiction coefficient and potential significantly correlated to the formation and breakdown of the oxidation layer. A model is then proposed for the explanation of the phenomena and the mechanisms.**

I. INTRODUCTION

The survey method of material wear is very important for the study of properties of material abrasion. Usually abrasion resistance of a material is determined by surveying the length change, weight change or volume change of the sample before and after abrasion test[1-3]. All of these methods have the same characteristic, which expresses the material abrasion level through the change between initial state and final state of the test sample. These methods, however, do not produce almost any information from abrasion process.

Tribo-electrification is a well-known physics phenomenon and this effect has something to do with the friction process[4-9]. The present work concentrates on the effect of electric potential varying with the abrasion condition in the test specimen. It is found that the test specimen can produce different electric potential which vary in pattern in different wear conditions, such as different friction speed, different abrasive size and different specimen which differ in metallographic structure. By this way, the information of materials abrasion would be found dynamically.

II. Procedure for Paper Submission

A. Sample Preparation

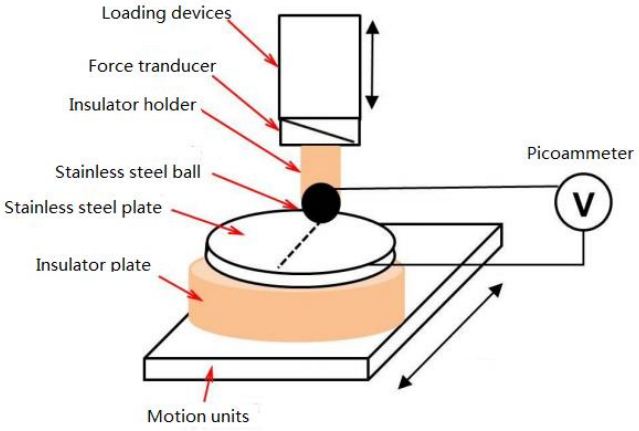

Figure 1. The schematic diagram of the friction test

Fig.1 shows the schematic diagram of the measuring process. The upper samples were 4mm diameter commercial stainless steel balls (C 5.5% Cr 2.2% Fe 91.4%), the surface roughness of which was below 14nm. The counterpart samples were 24mm diameter stainless steel plate(C 5.4%, Cr 17.8%, Ni 8.2%, Fe 64.6%). The plate was well polished in order to control the surface roughness and surface oxygen layer thickness. The mechanical properties of the specimens are listed in Table.1.

Table 1. The mechanical properties of the frictional pair

	Bearing Ball	**Stainless steel plate**
Compositions	C 5.5% Cr 2.2% Fe 91.4%	C 5.4%, Cr 17.8%, Ni 8.2%, Fe 64.6%
Dimensions	D=4mm	D=24mm, H=4mm
Yield strength/MPa	1600	205
Elastic modulus/GPa	207	180

The stainless steel plates were polished before the experiment. The polishing process started with #200 abrasive paper and finished with #4000(plate B) and #2400(plate C). The duration time of polishing for each abrasive paper was set to be 12min. The surface roughness was then measured, as shown in Table.2. Plate A went through almost the same polishing process with plate B except that the duration time of #4000 was extended to 36min. The surface roughness of plate A and B were considered the same, but the thickness of the surface oxide layers were different, as shown in Table.2. The surface roughness was

measured by an interferometer, and the surface oxide layer was measured by an auger electron spectroscopy.

The specimens were ultrasonic cleaned with absolute ethyl alcohol and acetone for 10min each, and dried with 70℃ drying oven.

TABLE 2. SURFACE PROPERTIES OF THE PLATE SAMPLES

	Plate A	Plate B	Plate C
Surface roughness/nm	43.3±7.2	43.4±14.1	101.1±25.7
Oxide layer thickness/nm	3.6	2	2.8

B. Friction Test

The basic experimental idea is to survey the electrical potential during wear. Fig.1 shows the schematic diagram of the measuring process. Friction test was made on a friction test apparatus under isolated circumstances. The stainless steel plate was driven by a motor and moved reciprocatingly. Typical electrostatic potential curve was obtained in ambient environment (23℃， 30% humidity). The normal load varied from 0.5N to 4N, and the average sliding speed varied from 0.5mm/s to 4mm/s. The friction test lasted for 30min.

The friction coefficient was measured by a cantilever beam transducer, the in situ electrostatic potential was measured with a picoammeter (Keythley 6514), and the wear track was observed by a scanning electron microscope.

III. RESULTS

A. Typical potential curve with friction coefficient

Typical electrostatic potential curve was obtained with 1N of normal load, 2mm/s of sliding speed on plate B.

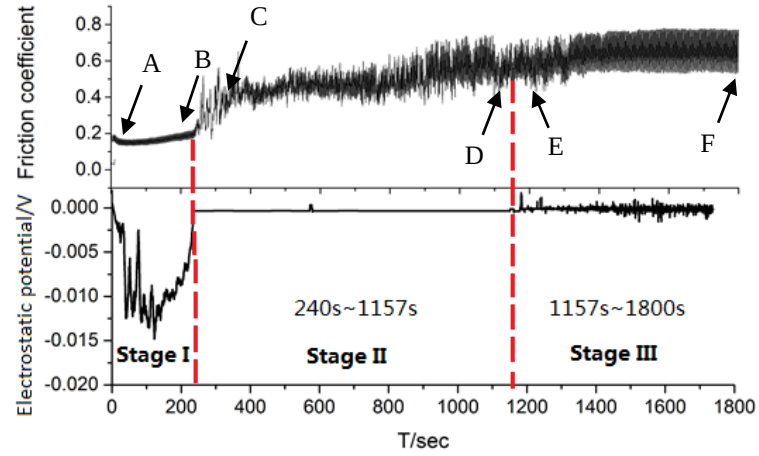

(a)

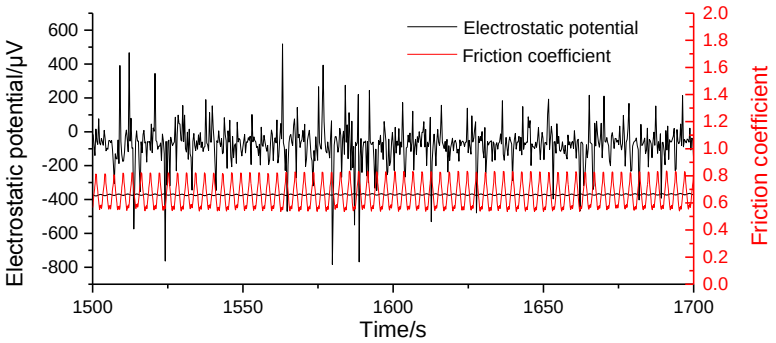

(b)

Figure 2. The typical potential curve with friction coefficient. (a) 30min friction test and (b) detailed potential curve in stage III

Result shows a direct correlation between electrostatic potential and friction coefficient. The friction process can be divided into three stages with different features of both friction coefficient and electrostatic potential, as shown in Fig.2.

Stage I (from 0 to 240s): The friction coefficient remains relatively low and stable (below 0.2, the average value is 0.18), and the potential of mV order is recorded. The potential remains negative as measured, and reaches the maximum of -7mV at 123s. At

240s, the potential abruptly decreases while the curve of friction coefficient starts to oscillate and increase.

Stage II (from 240s to 1157s): The average coefficient escalates from 0.2 to 0.6 as the friction goes on. The electrostatic potential oscillates around zero and partially negative, the maximum value of potential is in the order of several microvolts.

Stage III (from 1157s to 1800s): The average coefficient gradually reaches 0.65 and remains unchanged, while the oscillation of the coefficient is even more severe than stage II. The potential shows the same trend as stage II, only the value is two orders of magnitude higher and reaches a maximum of -787 microvolts, as shown in Fig.2(b).

B. Morphology of the wear

The SEM morphology of the wear track of the specimen in section 3.1 has been observed at the beginning and end of every stage (marked as A-F in Fig.2(a)), as shown in Fig.3.

In Fig.3(a)-(b), there is no obvious wear debris observed in the wear track both on the bearing ball and the plate, especially in Fig.3(a), which means the beginning of the friction process. The ploughing in Fig.3(a) and (b) mainly due to the plastic flow of the surface layer. As the friction goes on, the surface layer of the stainless steel plate is damaged, the lamella debris is attached on the upper sample (in Fig.3(c)). At this point, the potential decreases to almost zero, and it can be deduced that this abrupt change may due to the breakdown of the surface layer.

At the end of stage II (see Fig.3(d)), powdery debris occurs on both of the friction pairs, and the distribution of debris on the upper sample is discontinuous, EDX results indicates both inside and outside layer debris is consist of material from the plate . The wear track on the plate is measured to be 300μm on the morphology, and the wear debris is dispersive in and out of the wear track.

Fig.3(e) and (f) represents stage III. The discontinuous distribution of debris on the upper sample still exist, but the outside layer debris mainly comes from the plate, while the inside layer debris from the stainless steel ball according to the EDX, which means the debris of each friction pair is separated. It can also be observed that the wear debris accumulates along the wear track, thus the debris inside the wear track is far less than stage II. At the same time, signs of adhesion and oxidation are observed inside the wear track, which indicates the reason for the potential change between stage II and III. Detailed explanations will be made in Section IV.

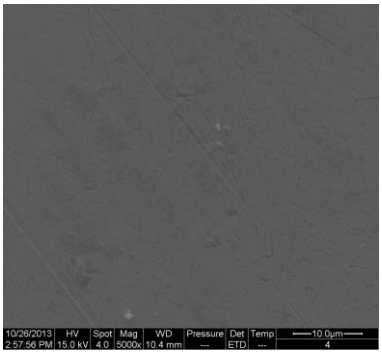

(a-1)

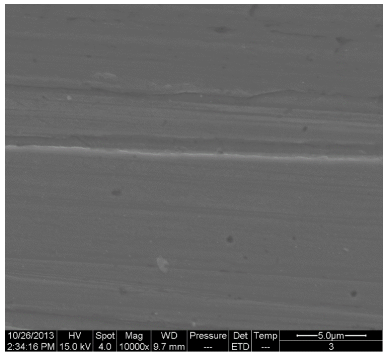

(a-2)

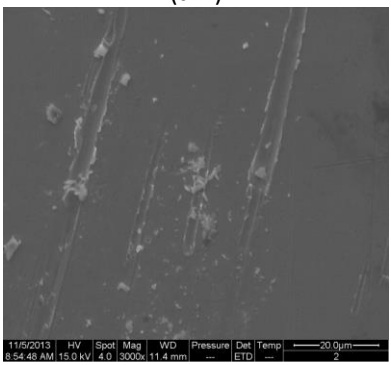

(b-1)

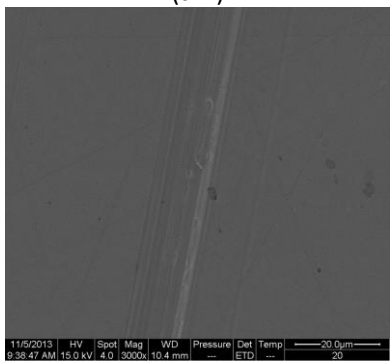

(b-2)

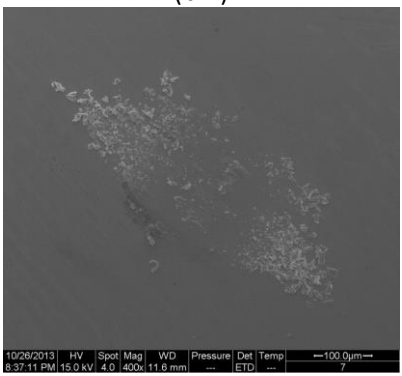

(c-1)

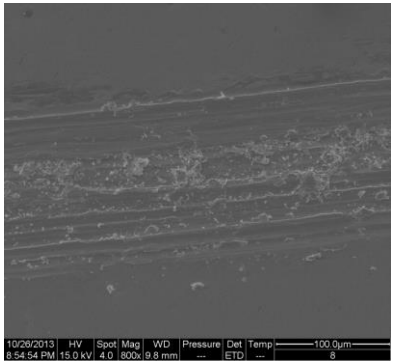

(c-2)

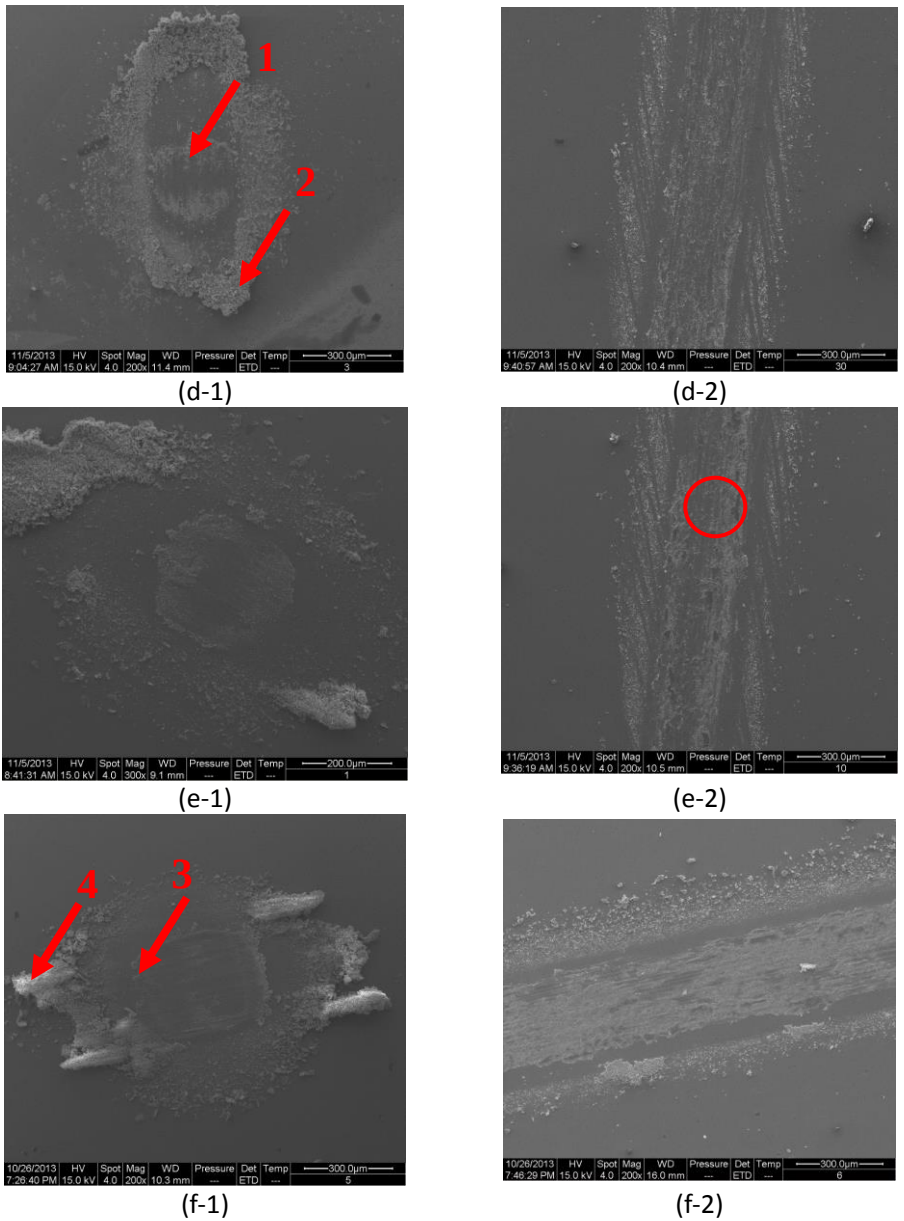

Figure 3. The SEM morphology of the friction surface. (a) to (f) stand for the A-F marked in Fig.2(a). Pictures of the left column are the morphology of the wear scar on the bearing ball, and the right ones are that of wear track on the plate.

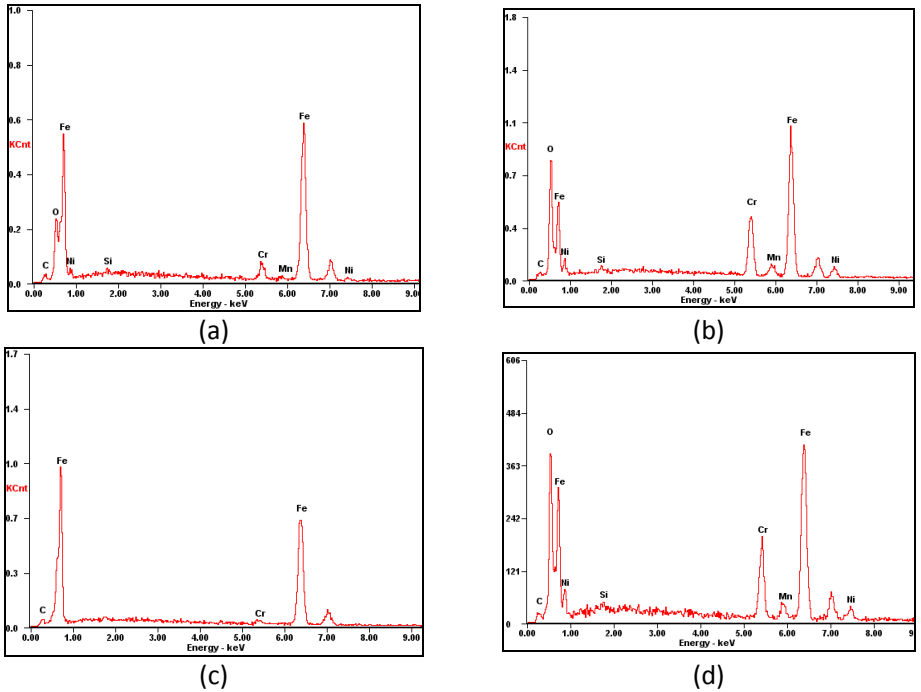

Figure 4. The EDX analysis for the wear debris on bearing balls. (a) and (b) is for the marked 1 and 2 in fig.2(d-1), (c) and (d) is for the marked 3 and 4 in fig.2(f-1).

C. The influence of external conditions

Friction tests of different external conditions on plate B are made. Fig.5 and 6 shows the influence of normal load and sliding speed on the friction potential (Stage I). Both the duration time and the maximum potential value of stage I shows a monotonous variation with the normal load, but not with sliding speed. As shown in Fig.6, the largest electrostatic potential occurs at the sliding speed of 1mm/s.

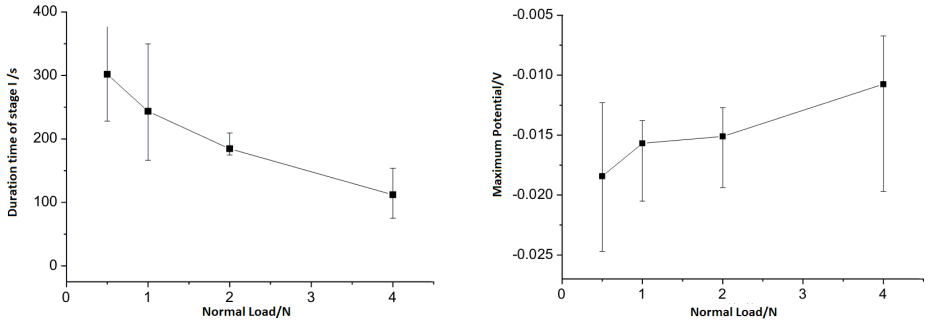

Figure 5. The influence of normal load on (a) duration time of stage I and (b) maximum potential value of stage I

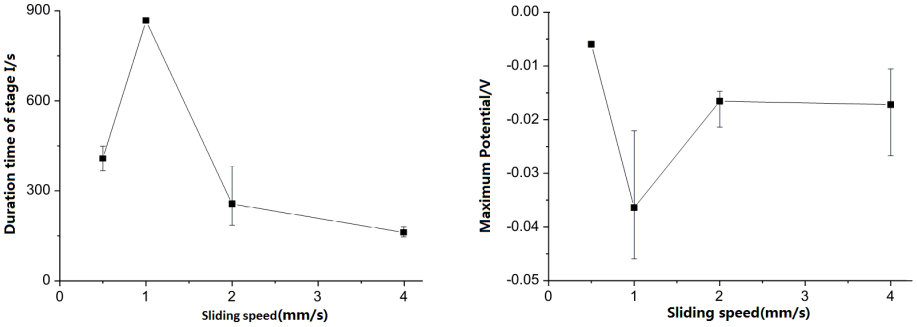

Figure 6. The influence of sliding speed on (a) duration time of stage I and (b) maximum potential of stage I

D. The influence of surface conditions

Friction tests of different surface conditions are made (See Fig.7). The normal load is 1N, and the sliding speed is 2mm/s. According to different polishing process, the three plate samples exhibit different surface properties. The surface roughness of plate B and C are different, the one with smaller surface roughness accumulates more net charge in stage I. Plate A and B have different surface oxide layer thickness while the roughness could be considered the same. Plate A, with thicker oxidation layer, accumulates more net charge compared with plate B.

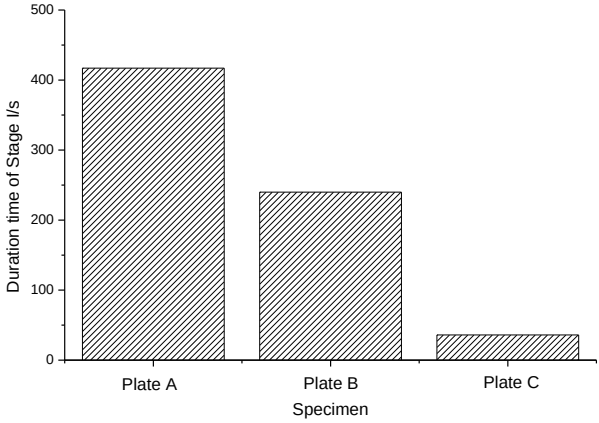

Figure 7. The influence of surface properties on duration time of stage I.

IV. DISCUSSIONS

It is obviously seen from the experimental results that the electrostatic potential is correlated with the oxidization of the contact surface. A model is then proposed considering the surface asperity and oxidation layer.

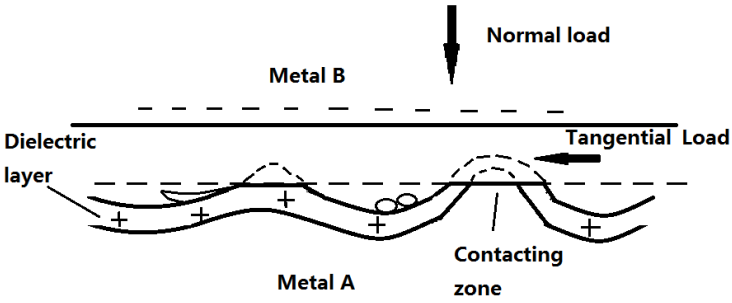

Figure 8. Model of tribo-electrification of dielectric layer.

As shown in Fig.8, the carbon steel surface is covered with a several nanometers of oxide layer and absorbed layer, which could be considered as dielectric layer. In the beginning of the friction, it causes more charges to be generated on the tribo-surfaces of frictional pairs under a good contact condition (more smooth surfaces), thus enhancing the charge transfer. Simultaneously, the rapid separation after friction will cause the surface charges to flow and arrange anew quickly. As a result, the charge quantity in dynamic equilibrium is stored on the interfaces of frictional pairs and, hence, a relatively stable tribo-electrification electrostatic potential can be determined.

When the asperity is broken off due to the strong adhesion, the dielectric layer is broken down, and the metal-metal contact takes place. The charge transfer still exist but there will be no accumulation of the transferred charge, thus the measured value of the potential is almost zero.

The experimental results of surface roughness and oxide layer thickness verify this hypothesis. On one hand, the asperities on rougher surface has a lower elastic-plastic deformation resistance during the friction [10], thus the breakdown of the surface layer is easier to take place compared with the smoother ones. On the other hand, the thickness of surface layer affected the breakdown time directly.

After a certain time of friction, the heat accumulates in the metal-metal interface and causes the adhesion of the two frictional pairs, along with new oxide layer generated in the real contact zone. The oxide layer will not be continuous and will be soon worn off after the formation. The wear debris of the newly generated oxide will adhere to the opposing specimen. Since the free electrons are excited during the material transfer, the wear debris usually has negative electricity, and as a result, the plate will be positive in potential. Thus

the large oscillation of electrostatic potential and friction coefficient in stage III can be attributed to the balance of oxidation formation and removal.

V. Conclusion

Under point contact dry sliding, an obvious change on magnitude of the tribo electrification electrostatic potential of bearing ball and stainless steel plate could be observed correlating with the friction coefficient tendency. After stainless steel plate rubbing against the bearing steel, the tribo-electrification electrostatic potential was not constant, and it will abruptly drop from several mini volts to almost, especially under severe sliding conditions. The positive charge existed on the tribo-surface of bearing ball and the negative charge existed on the tribo-surface of the plate.

During severe wear process, the experimental conditions, the surface roughness, the surface oxide layer thickness, and the fraction of surface film in the contacting zone were the most significant interaction effects on the abrupt change in tribo-electrification electrostatic potential.

A model is then proposed for the tribo-electrification mechanism. The existence of the surface dielectric layer guarantees the low and stable friction coefficient and large measured potential in the beginning of the friction process. The breakdown of such dielectric layer leads to the abrupt change of electrostatic potential. And the large oscillation of electrostatic potential and friction coefficient in stage III can be attributed to the balance of oxidation formation and removal in the real contact area during the friction.

References

[1] J. Salib, Y. Kligerman, and I. Etsion: "A Model for Potential Adhesive Wear Particle at Sliding Inception of a Spherical Contact", Tribology Letters, vol. 30, 2008 pp. 225-233.

[2] H. Unal, S.H. Yetgin, A. Mimaroglu and M. Sumer, "The Effect of Test Parameters on Friction and Wear Performance of PTFE and PTFE Composites", Journal of Reinforced Plastics and Composites, vol.29, 2010, pp:1978-1986

[3] A. Amanov, et al, "Fretting wear and fracture behaviors of Cr-doped and non-doped DLC films deposited on Ti–6al–4V alloy by unbalanced magnetron sputtering", Tribology International, vol.62. 2013, pp: 49-57

[4] L.Q. Jian, L.P. Ning, S.G Yang, J.M. Wang, "Triboelectrification Electrostatic Potential of MC Nylon 6 under Point Contact Dry Sliding" , Tribology Letters, vol. 36, 2009, pp:199–208,

[5] Y C Chiou, Y P Chang, R T Lee. "Tribo-electrification mechanism for self-mated metals in dry severe wear process". Wear, Vol.254(7-8), 2003, pp: 606-624.

[6] Y C Chiou, Y P Chang, R T Lee. "Tribo-electrification mechanisms for dissimilar metal pairs in dry severe wear process". Wear, vol. 264(11-12), 2008, pp:1085-1104.

[7] S Morris, R Wood, T J Harvey, et al. "Electrostatic charge monitoring of unlubricated sliding wear of a bearing steel". Wear, vol.255, 2003, pp:430-443.

[8] L P Ning, L Q Jian, S R Yang, et al. "Effect of carbon black on triboelectrification electrostatic potential of MC nylon composites". Tribology International, vol.43, 2010, pp: 568-576.

[9] J Tang, L He, Z H Jin , et al. "Material tribo-electrification potential changing during wear. " Materials & Design, vol.24, 2003, pp: 223-226

[10] W.R. Chang, I. Etsion and D.B. Bogy: "An Elastic Plastic Model for the Contact of Rough Surfaces. J. Tribology", Trans ASME, vol. 109, 1987, pp. 257-263.